

To appear in the *Astrophysical Journal*

Infrared Photometry of Starless Dense Cores

D C. Murphy

Carnegie Institution of Washington, 813 Santa Barbara St., Pasadena, CA 91101

david@ociw.edu

P C. Myers

Center for Astrophysics, 60 Garden St., Cambridge, MA

pmyers@cfa.edu

ABSTRACT

Deep JHK_s photometry was obtained towards eight dense molecular cores and J - H vs. H - K_s color-color plots are presented. The results of our photometry indicate that these cores are free of embedded stars down to the hydrogen burning limit and free of brown dwarfs down to the 10M_{Jup} limit. Optical extinctions are estimated for the detected background stars, with high extinctions being encountered, in the extreme case ranging up to at least A_V = 46, and probably higher. The true core maximum extinctions are probably larger as our estimates are lower limits. The extinction data are used to estimate cloud masses and densities which are comparable to those determined from molecular line studies. Variations in cloud extinctions are consistent with a systematic nature to cloud density distributions and column density variations and extinctions are found to be consistent with submillimeter wave continuum studies of similar regions. The results suggest that some cores have achieved significant column density contrasts (> 30) on sub-core scales (< 0.05 pc) without having formed stars or brown dwarfs.

Subject headings: stars: formation { ISM : clouds { ISM : globules

1. Introduction

The first near infrared (NIR, $\lambda = 1 - 2.5$ m) observations of dark clouds were toward the Ophiuchus dark cloud complex by Grasdalen, Strom, and Strom (1973), who interpreted their observations as revealing the presence of an embedded star cluster. Pioneering studies such as this were hampered by their inability to distinguish between background field stars and embedded PM S stars, as well as by their comparative lack of sensitivity compared with modern IR array based observations. Despite these problems, these initial surveys were able to detect small numbers of PM S objects in dark cloud regions, evaluate the reddening laws, and place lower limits on cloud dust extinctions. Visual extinctions for dark cloud complexes were typically found to be ~ 10 (Elias 1978a,b; Hyland 1981). Hyland (1981) reviewed the early work in this field and discussed the use of the $J - H$ vs. $H - K$ color-color plot as a powerful technique to discriminate PM S stars from field stars, laying the ground work for modern studies. The advent of NIR imaging brought a new impetus to NIR studies of dark clouds. Extensive surveys of cooler dust clouds, some known regions of low to intermediate mass star formation have now been performed. These surveys have studied the embedded stellar content, probed the IMF, revealed the presence of brown dwarfs, and probed the mass distribution of molecular clouds (Evans 1999; Lada, Alves, and Lada 1999a; Lada 1998; Wilking 1997; Lada 1990). NIR photometry has proven to be an effective method for probing the internal mass structure and stellar content of dark clouds. Compared with longer wavelength IR observations, the NIR combines wide field coverage, ground based telescope aperture and accessibility, with acceptably low sky/telescope background. The resilience of NIR photometry to reddening is also excellent, especially in the K_s passband ($\lambda = 2.25$ m), where $A_K - A_V = 11$.

Most studies to date have concentrated on wide area, low sensitivity surveys of large star cloud molecular complexes or in some instances individual optically cataloged Bok globules, while fewer systematic surveys of dense molecular cores in the IR have been made. We present here the results of sensitive ($K_s = 17.2 - 19.8$) NIR observations of dense cores found in dark clouds. These cores are lacking in associations with optically identified young stellar objects or embedded IRAS sources.

An abundance of evidence now indicates that galactic star formation occurs in cold ($T = 10 - 20$ K) dense ($n = 10^4$ cm⁻³) molecular cores either found as components of larger molecular cloud complexes or as isolated dark clouds. Dense cores are identified by surveying these clouds in radio and millimeter spectral lines that trace dense molecular gas such as NH₃ and C₁₈O (Myers, Linke, and Benson 1983; Benson and Myers 1989). Clear evidence exists that these regions represent a link to the earliest stages of star formation. For instance, dense cores are often found in close proximity to groups of T-Tauri stars. More directly, some

dense cores are known to have embedded young stellar objects (YSO's) or other indicators of embedded young stars. Star formation tracers associated with dense cores include class 0 and 1 IRAS sources, H II objects, H₂O masers, several types of emission line stars (or other low-mass stars with extreme spectral features and colors), and bipolar gas flows (Beichman et al. 1986; Jijina, Myers, and Adams 1999). Naturally one is led to conjecture that dense cores represent an early stage of star formation: that of a self-gravitating mass, portions of which are collapsing or have recently collapsed to form stars.

If such stars are undergoing gravitational collapse, the spectral signature for a line of modest optical depth ($\tau \approx 1$) is that of an apparent blue-shifted profile (Hummer and Rybicki 1968). Observations of YSO's and class 0 IRAS sources (often associated with dense cores) have shown significant excess of blue-shifted spectral profiles indicating a significant population of sources with inward motions (Zhou et al. 1993, 1994; Myers et al. 1995; Gregerson et al. 1997; Mardones et al. 1997). Most YSO's are, however, also known to be associated with molecular outflows (bipolar flows), confusing the interpretation of spectral line data. Also, some observed in outflows may not be truly "star forming" as most of the stellar mass might have already been accumulated.

The molecular cores selected for study here are a small and special subset of the cores from the lists of Benson and Myers (1989) and Lee, Myers, and Tafalla (2001) and are of special interest as candidates for the very earliest stage of low mass star formation. Specifically, these objects have been selected according to the following criteria:

- 1) They are free known associations with optically visible pre-main sequence objects, and in fact most optically visible stars in their denser regions (as ascertained from Palomar Observatory Sky Survey Plates).
- 2) Most are not IRAS sources and have no other indicators of embedded star formation.
- 3) They have, in some cases, a spectral signature in millimeter wave transitions consistent with cloud gas infall. Five of the cores discussed here (L1689B, L183B, TM C1, TM C2, and L158) are classified as either "Strong Infall Candidates" or "Probably Infall Candidates" based a velocity analysis of extensive mapping in the CS (2-1), N₂H⁺ (1-0), and C¹⁸O (1-0) lines (Lee, Myers, and Tafalla 2001).
- 4) They are well studied at other wavelengths, are relatively nearby (d \approx 450 pc), and have projected molecular core sizes well matched to the few arc minute scales of current NIR imaging cameras.

The objectives of our study here will be to:

- 1) Provide a further sensitive diagnostic of embedded stellar or brown dwarf content of

the dense cores allowing a less ambiguous interpretation of the gas velocity structure (i.e. infall vs. outflow) and clarifying the evolutionary state of these cores.

2) Measure the mass and density of the cores independent of methods based on molecular line observations which rely on numerous assumptions regarding molecule and grain chemistry, excitation physics, and radiative transfer.

3) Provide information on the spatial distribution and organization of the core gas in terms of central concentration and clumpiness.

2. Observations and data reduction

The observations were carried out in two observing runs at the 1 m Swope Telescope at Las Campanas Observatory, Chile, and one on the 60 inch telescope at Palomar Observatory. Infrared cameras utilizing the Rockwell NICMOS3 256 X 256 HgCdTe array were used. The camera used for the 60 inch telescope observations is an Onewrimager based, all reflective design described in Murphy et al. (1995). The infrared camera used on the 1 m Swope telescope is also an Onewrimager camera very similar in design to that described in Murphy et al. (1995) differing only in optical details primarily related to the fact that it is deployed on a telescope with a different focal ratio. The field-of-view (FOV) and plate scale of both cameras is nearly the same at 2.6' X 2.6' and 0.60" pixel⁻¹, respectively. Table 1 summarizes the observational parameters.

Frames at J;H, and K_s were obtained for all core positions, with typical integration times of several hundred seconds per filter, per core. The core positions (Table 2) were taken from the peaks of NH₂⁺ and NH₃ emission line maps, both tracers of dense gas and velocity structure diagnostics. In the cases of L1709A and L1696B (which don't have published maps), the center of the IR frame is estimated to be approximately 50" east and 70" northeast of the published NH₃ positions, respectively, as these positions better define the overall the optical core. The final JHK_s images are elongated N-S from the intrinsic 2.6' X 2.6' camera fields by 10-40" as the telescope was dithered N-S a few times per color so that sky frames could be built from the data themselves as is standard with IR imaging. Twilight flats were taken at sunset and sometimes sunrise, and standard stars taken from Persson et al. (1998) were systematically observed throughout the night. Dark frames were taken for all integration times used, usually at the beginning and end of the night, as well as during the night if time allowed (such as just after a standard star measurement). The seeing ranged from 0.9 - 2.0" (FWHM), depending on the telescope, site, airmass, and night, with typical values being close to 1" for the Las Campanas observations and 1.5" being typical for the

poorer Palomar 60 inch site.

The data were reduced using IRAF and a standard set of scripts developed for this purpose at the Carnegie Observatories. All data frames were first linearized. Following this, all dark frames and frames taken at the same position in the sky were averaged with a sigma-clipping algorithm turned on to eliminate cosmic ray hits. Averaged dark frames were then subtracted from all data frames and the resultant dark-subtracted images were aligned using normalized twilight flats.

An iterative approach to sky subtraction was used to reduce the data. The point of the iterative operation is to suppress the residual stellar artifacts that would remain on a sky frame after conventional direct medianing, thus improving the accuracy of stellar photometry. Starting with the dithered images across each core position, i.e. linearized dark-subtracted attened images, sky-subtracted mosaics were created by the following process. A median averaged sky frame was formed from all dithered images. This now star-free sky frame was further attened with SExtractor to form a first order sky (Bertin and Arnouts 1996). This first order sky was subtracted from each dithered image frame to produce reduced first order dithered images. Stars were then identified interactively on each of these reduced first order dithered images and their (x; y) positions logged a disk file. The second iteration of the mosaic creation process begins by returning to the dithered images and using the saved (x; y) stellar positions to clean them of stars to form star-free dithered images. This second pass used a script based on the IRAF task imedit. The star-free dithered images were then medianed to obtain a nalsky for each core at each color. Finally, the nalsky was subtracted from the original dithered images, the resultant images were aligned and shifted using a fiducial reference star and sigma-clipped averaged to form a nalm mosaic at the core position. In a few cases the nalm mosaic was further processed by SExtractor to remove residual curvature.

The standards calibration was applied to each nalm mosaic and aperture photometry performed by hand on individual stars using an IRAF script based on the IRAF phot routine. The brightest stars in a clean area of the frame were generally used to define the PSF for aperture photometry, although in cases where bright stars were not present, the PSF was determined from bright stars on the frames of other sources observed on the same night (at the same color). The errors in the photometry are dominated by systematic errors in the PSF and the PSF fitting procedure which was performed (by inspection) on a star-by-star basis. The conservatively estimated errors in the photometry are a quadrature combination of the statistical measurement error and the estimated error in the PSF determined individually for every star.

3. Results

The data are presented in the form of tables summarizing the photometry, processed in images at each color, and $J - H$ vs. $H - K_s$ color-color diagrams.

Table 2 lists the approximate center positions of the individual image mosaics given in Figures 1-4 and their value in J2000.0 coordinates. The positional errors for the 1 m Swope observations ($10''$) are higher due to the poorer pointing accuracy of this telescope, and bearing in mind that optical reference stars in the fields are not available because of the generally star-free nature of the sources.

Tables 3-10 summarize the photometry for each source. The columns give a running number identifying each star, the $JH - K_s$ magnitudes, $J - H$ and $H - K_s$ colors, and a reddening measure. Five sigma lower limits are estimated for each magnitude and color and are given in the table columns or in the captions. In some cases the limiting magnitudes are fainter for redder colors despite the fact that observations at redder colors in the NIR are less sensitive due to higher background for the same integration time. This reversal of the normal state-of-affairs was due to the lack of detectable stars at J or H , meaning that dithered frames could not be stacked together so that integration times at these bluer wavebands were less. Photometry and colors for a particular star are not given if for some reason a reliable value could not be obtained from the data, such as if the star is beyond or at the edge of the mosaic (specifically noted) or for any other reason a PSF fit could not be obtained (denoted by ellipsis in the table entries). The stars in Tables 3-10 are identified in Figures 1-4 on the image mosaic used for that purpose, usually the K_s mosaic.

The last column of Tables 3-10, the reddening measure $A_V (K_5)$, is an attempt to provide a relative measure of the core reddening. Calculated here is the optical extinction assuming that the typical background star is K5 main sequence (MS). Following the reddening law of Koomneef (1983), this is taken to be

$$A_V (K_5) = 15.385 E (H - K); \quad (1)$$

where $E (H - K)$ is the color excess given by

$$E (H - K) = (H - K) - (H - K)_{K_5}; \quad (2)$$

Deriving $(H - K) = 0.16$ from Table 3 of Koomneef (1983), we obtain

$$A_V (K_5) = 15.385 [(H - K) - 0.160]; \quad (3)$$

This calculation is also performed for stars that have only $J - H$ lower limits and in such case would be a meaningful quantity if the star was field type as opposed to being embedded

in the cloud. We note that the seemingly simplistic assumption that the typical background star is a K 5 with $H - K = 0.16$ actually introduces a maximum error of only 2.3 magnitudes into the extinction estimate given by (3). This is because the intrinsic range of $H - K$ values for dwarfs and giants for spectral types A 0 to M ranges only from 0.0 to 0.3 magnitudes (Koornneef 1983). A detailed discussion of this issue is given by Alves et al. (1998) and Lada et al. (1994). By way of example, these authors measured extinction free comparison fields for the dark clouds IC 5146 and L977 yielding $H - K = 0.13 \pm 0.01$ and $H - K = 0.20 \pm 0.13$, respectively.

Figures 5-12 give $J - H$ vs. $H - K_s$ color-color plots for each core. The MS and reddening vectors of Koornneef (1983) are plotted on each diagram. Following Lada and Adams (1992) we have marked the reddened positions of stars projected on the MS at $A_V = 5, 10, 15, 20, 25$, and 30 (where applicable) with X's. Lada and Adams (1992) provide a detailed observational and theoretical classification of YSO's in the $J - H$ vs. $H - K_s$ color-color plane. Lower limits (or in a few cases upper limits) on colors are indicated by arrows along the direction of the undetermined color. These are mostly lower limits on $J - H$. In these plots, and all calculations, we have assumed that $K_s = K$ which will introduce a negligible error in our analysis, particularly in light of the other uncertainties in the photometry, reddening law, and intrinsic spectral nature of the detected stars (Persson et al. 1998; Rubio et al. 1998). The individual objects are discussed in detail in the following sections.

3.1. L1709A

Of the cores discussed here, L1709A had the most number of stellar objects detected in the IR: Colors or limits are presented for 39 stars in Table 3. Figure 1 displays the $JH - K_s$ mosaics and identifies the stars.

This core, despite its complete absence of optically identified stars on the digitized Palomar Observatory Sky Survey (POSS), exhibits stars in the infrared and shows an excess of stars with increasing infrared wavelength. The color-color plot Figure 5 indicates that nearly every star with plottable colors has colors consistent with being a reddened field star. The one possible exception is IR 11 which is in a region of the color-color plot consistent with it being a classical T-Tauri star (CTTS) just slightly to the right of the reddened MS. We note that even this result is suspect since this data point has large error bars. The reddening measure (Table 3, col. 7) indicates that the L1709A stars range from unreddened to $A_V (K 5) = 23.6$ with $\langle A_V (K 5) \rangle = 12.2$.

3.2. L1582A

L1582A was the second most populous object in terms of the number of stars detected. Colors or limits are presented for 17 stars (Table 4). Figure 1 displays the JH K_s mosaics and identifies the stars.

As with L1709A, this core displays numerous visible IR stars increasing in number with wavelength, despite the fact that only two visible stars are detected on the POSS. The color-color plot Figure 6 indicates that all stars with plottable colors but one, IR 5, have colors consistent with being field or reddened field stars. IR 5 is in the classical T-Tauri star region (CTTS) of the color-color plot consistent with it being a young stellar object (Lada and Aladams 1992). We note that this result is somewhat in doubt since this star is near the edge of the K_s frame, probably degrading the quality of the photometry. The reddening measure for L1582A (Table 4, col. 7) varies from $A_v = 1.5$ to 27.9.

3.3. L158

This core is devoid of stars on the POSS, but may be associated with the class I IRS source 16445-1352, located approximately 2' north of the molecular core center position and at the projected northern edge of the core. This IRS source is 30" north of the northern boundary of our IR frame (Lee, Myers, and Tafalla 2001; Bouy et al. 1996). Stars are seen in our N IR frame with colors or limits being provided for eight stars in Table 5. Figure 2 displays the JH K_s mosaic and identifies the stars.

The six plottable stars on the color-color diagram Figure 7 indicate field or reddened field stars except IR 6 which displays colors consistent with it being a CTTS. We note however, that IR 6 has very large error bars and is faint. Furthermore the $H - K_s$ error bar is nearly consistent with it being on the reddened main sequence. The JH K_s frames clearly show a greater visibility of stars with increasing wavelength. The reddening measure ranges from A_v (K 5) = 1.0 to 34.3 (Table 5, col. 7).

3.4. TM C 1

In the literature, TM C 1 is often considered associated with the class I IRS 04381+2540 although we note that this object is 6' west and 1.8' north of the molecular core center position and well outside the boundary of our IR observations (Handler, Barsony, and Moore 1998). Several stars are detected in our N IR frame, with colors or limits being given

for given 11 stars in Table 6. Figure 2 displays the JH K_s mosaics and identifies the stars.

The nine plottable stars on the color-color diagram Figure 8 indicate that all stars have colors consistent with being highly reddened old stars although definitive statements cannot be made regarding stars with J - H lower limits. The three stars found at the rightmost portion of the color-color diagram with J - H lower limits are either highly reddened old stars, or PM S stars judging from the colors alone. The JH K_s images show a greater visibility of stars with wavelength, in fact only two stars had measurable J magnitudes. The reddening measures ranged from 12.6 to an astonishing 46.2.

3.5. L1696B

Colors or limits are presented for 12 stars towards the L1696B core (Table 7). Figure 3 identifies the stars and displays the H and K_s mosaics (no stars were detected at J).

Of the six plottable stars on the color-color diagram of Figure 9, two are clearly consistent with being old stars, while four are either very reddened stars or remain sequence objects judging from their colors alone. As is typical with all the cores, the images show a greater visibility of stars with wavelength. The reddening measures range from 18.4 to 36.0.

3.6. L134A

Colors or limits are presented for three stars towards the L134A core (Table 8). Figure 3 identifies the stars and display the H and K_s mosaics (no stars were detected at J).

All three stars are plotted on the color-color diagram Figure 10 as points with J - H lower limits. Technically these are either remain stars or highly reddened old stars. The reddening measures for these stars are 18.8, 16.5, 24.4.

3.7. TMC 2

Colors or limits are presented for seven stars (Table 9) towards the TMC 2 core. Figure 4 identifies the stars and displays the H and K_s mosaics (no stars were detected at J).

Only three of the stars were plottable on the color-color diagram (IR 3, IR 6, and IR 7) and these only with J - H lower limits making their nature uncertain (Fig. 11). The reddening measures for these stars are 33.9, 23.4, and 26.6 for IR 3, IR 6, and IR 7, respectively.

3.8. L183B

Colors or limits are presented for three stars towards the L183B core (Table 10). Figure 4 identifies the stars and displays the H and K_s mosaics (no stars were detected at J).

Only one star (IR 3) was plottable on the color-color diagram, and although it only has a J - H lower limit, its colors are consistent with it being a reddened field star (Fig. 12). This core is the closest to being truly free of any associated stars of the sources studied here, displaying no detections at J and only one star in the H frame. IR 3 has a reddening measure of 9.7.

4. Discussion

These dense cores, all initially considered to be nearly star-free in the optical and IRAS data, have in fact been shown to have numerous near infrared stellar detections projected at or near their centers. This result indicates the marginal utility of relying on survey optical plates to identify star-free dust clouds.

The color-color plots of these stars indicate, in the case where all three magnitudes are available, that nearly all have colors consistent with field stars, often highly reddened ones. Three stars discussed above have colors possibly consistent with an identification as PMS objects, but the evidence for this is very weak as these stars have, in all cases, arguably underestimated photometric errors. Reobservation of these stars, and if necessary, infrared spectroscopy on a large telescope could clarify this situation. There is no evidence of any substantial embedded stellar population in any of the sources (such as a star cluster).

The mean extinction measure as defined above is tabulated for each case in Table 11. To the extent that this measure indicates a reasonable indication of cloud optical extinction one can say that core extinctions range from 10 to about 30 magnitudes with a grand average of 19.4. The largest mean extinction was towards TMC 1 (30.3), which also had the most reddened star IR 7 with $A_V (K_5) = 46.2$. Deeper and longer integrations on larger telescopes will be necessary to penetrate to the inner regions of these cores in the near infrared. These substantial extinctions clearly underestimate the true core extinctions, since, as is evident from the mosaics in Figures 1-4, the detected stars strongly avoid the central regions of the cores. Our measured peak extinctions are a factor of 10 higher than that determined by optical star counts of dark cloud regions and a factor of 2-4 higher than that for the self gravitating, but non-starforming globule B 68 recently surveyed to its core in the NIR (Alves, Lada, and Lada 2001; Cernicharo and Bachiller 1984). Furthermore, our extinctions tend to be slightly higher than the wide area NIR extinction surveys of IC 5146

and L977 (Lada, Alves, and Lada 1999a). Our extinctions are generally comparable to, or less than absolute extinction values found in starless prestellar cores from submillimeter-wave continuum surveys, consistent with the fact that our values are lower limits (Ward-Thompson, Motte, and Andre 1999; Visser, Richer, and Chandler 2001).

The IR data allows us to estimate a lower limit to the core densities for six cores where a clear boundary was defined on K_s images by the outermost stars. The area of a polygon formed by these stars was calculated using core distances from Jijina, Myers, and Adams (1999) and Lee and Myers (1999). The ordered star list forming the polygon boundary for each core is given in Table 12. The geometric core radius A_p was divided into the core extinction measure from Table 11, and then multiplied by the standard factor of $0.95 \cdot 10^{21} \text{ cm}^{-2} \text{ mag}^{-1}$ (taking $A_V = 3.1E(B-V)$) to obtain an estimated lower limit on the total density of $H_2 + H$ (Bohlin, Savage, and Drake 1978). This method also allows a rough estimate on the core mass lower limit given by $n_{\text{tot}} A^{3/2} m_{H_2}$, where m_{H_2} is the mean mass of an H_2 molecule in the ISM, taken to be 2.72 times the mass of the hydrogen atom. The results of these calculations are given in Table 12. The densities, masses, and radii are all typical of dense cores in dark clouds. The density lower limit for L1582A is in agreement with the value of $1.6 \cdot 10^4$ of Jijina, Myers, and Adams (1999) determined from centimeter-wave NH_3 inversion line data, while our density for L158 is an order of magnitude higher than the Jijina, Myers, and Adams (1999) value. Considering that our densities are lower limits, the L158 result is unlikely to be due to geometric uncertainties, suggesting a possible breakdown of NH_3 molecule as a probe of these high densities. Similar effects have been reported for $C^{18}O$, which is found to be correlated with A_V only up to $A_V \approx 10$ (Kramer et al. 1999).

Given the fact that we do not image all the way through the cores to background stars at K_s , it is reasonable to consider how likely a very faint low mass T-Tauri star could, if located near the center of the cores, evade detection. Limits on this can be placed as follows. In Table 13 we have calculated the faintest detectable absolute K_s magnitude, M_K , detectable from a star located at the center of each core. This calculation assumes the extinction to the center is half the value given in Table 11 (taking $A_K = A_V = 11$), the detection limits of Tables 3 to 10, and distances from Jijina, Myers, and Adams (1999) and Lee and Myers (1999). Calculated M_K values range from 8.6 to 13.7. As to what can be expected from a low mass star, Zinnecker and McCaughrean (1991) have shown that at the low mass end of the IMF, $0.08 M_\odot$, M_K ranges from 4.9 to 5.3 M_\odot as the star descends the Hayashi track from ages $2 \cdot 10^5$ years to $2 \cdot 10^6$ years (see also Aspin, Sandell, and Russell (1994)). Thus, while not being able to absolutely rule out the existence of such an embedded star from our data, it is rather unlikely. Such an occurrence would require an improbable combination of circumstances. Take, for example, the case of L183B. Our simple model gives a detection

lim it 8.8 K_s magnitudes brighter than that needed to detect a 0.08 M_s star 2 10⁵ years old. This would mean that our A_v lower lim its would need to be a factor of 20 less than the actual extinction to miss such a star. Furthermore it would require that all potential embedded stars be at the lowest end of the mass spectrum, all be con ned strictly to the most dense regions of the cores, and all lacking an IRS-detectable luminous accretion disk.

Now that brown dwarfs are being detected in increasing numbers, it is interesting to ask if, while lacking clear evidence for associated stars above the hydrogen burning lim it, our cores might harbor young brown dwarfs. To put lim its on this possibility, consider a 0.01 M_s brown dwarf, an object corresponding to ten Jupiter masses. Weintraub et al. (2000) have shown that such an object declines from M_K = 8.3 to M_K = 10.8, between the ages of 10⁶ and 10⁷ years. According to our simple model, from Table 13 we see that such a brown dwarf would be detectable towards all our cores except the relatively distant L1582A in Orion. For L1582A the Weintraub et al. (2000) calculations show that a 0.02 M_s brown dwarf should be detectable, even with an age as old as 20 10⁶ years. We conclude that even if the A_v values of Table 11 greatly underestimate the extinction, the association of embedded young brown dwarfs with our cores is unlikely.

The estimated individual stellar extinctions in Tables 3-10 show considerable scatter, and generally speaking our data are too few to make detailed statements concerning the nature of the clumpiness of the extinguishing dust. This is natural of course as these sources were selected to be in star-free fields to begin with. For similar reasons it is not possible to make an estimate of cloud density profiles. However it is clear from Tables 3-10 and Figures 1-4 that column density density contrasts ranging from 1.5 - 34 exist in the clouds over scales of 0.05 pc, comparable to submillimeter continuum results (Ward-Thompson, Motte, and Andre 1999; Visser, Richer, and Chandler 2001).

In order to ascertain if such column density variations are random in nature or a result of under sampling a systematic density profile, we can further analyze L1709A and L1582A, the two cores with enough stars to perhaps make statistical arguments plausible and ask if our results are consistent with the study of Lada, Alves, and Lada (1999b) (and references therein). These studies consider $A_{v_{\text{mean}}} - A_{v_{\text{std}}}$ correlations, where $A_{v_{\text{mean}}}$ is the mean optical extinction calculated from all stars in a given projected area, and $A_{v_{\text{std}}}$ is the standard deviation in A_v for all stellar values in that same area. This relationship can be used to distinguish the true nature of the underlying continuous extinction, from undersampled data.

In an extensive study of the dark cloud IC 5146 employing 2000 stars, Lada, Alves, and Lada (1999b) found a linear ($A_{v_{\text{mean}}}, A_{v_{\text{std}}}$) relationship. This relationship has a slope dependent on spatial filter size. Taking the case relevant to our data set, a spatial filter of

90", these authors obtained

$$A_v = 1.0 + 0.41 A_v : \quad (4)$$

Here A_v is the mean standard deviation and A_v the mean optical extinction inside a 90" extinction map pixel. These authors do not give the error bars or intercepts of their fits for the 90" pixel case, so the intercept has been estimated from their Figure 13 and the intercept and slope errors are assumed similar to their equation 5, i.e. 0.11, and 0.01, respectively. This 90" filter case of Lada, Alves, and Lada (1999b) is the most relevant of their spatial filters to make a comparison with our data as it samples a significant fraction of the IC 5146 cloud. A similar relation, but with a slope of 0.40 ± 0.02 and intercept 1.93 ± 0.11, was obtained by Alves et al. (1998) for a sample of 1628 stars spanning a major fraction of the optically visible extinction towards the dark cloud L977. Applying the both the Lada, Alves, and Lada (1999b) and Alves et al. (1998) results to the A_v (K 5) values of Table 11 predicts $A_v = 6.0 \pm 0.8$ for L1709A, and $A_v = 5.6 \pm 0.4$ for L1582A. We calculate from all values in Tables 3 and 4, A_v (K 5) = 5.9 and A_v (K 5) = 9.2 for L1709A and L1582A, respectively. The agreement with the results of these authors is reasonable considering our small statistical sample.

Lada, Alves, and Lada (1999b) constructed a Monte Carlo density model for IC 5146 and showed that it could account for the measured A_v vs A_v relationship. This model consisted of a smooth, radially decreasing density gradient falling off as r^{-2} in a cylindrical cloud. Our agreement for the case of L1709A with the empirical A_v vs A_v relationship may indicate a similar smooth systematic density distribution.

5. Conclusions

We have studied 8 dense cores with deep JHK_s photometry in the NIR, the typical of which may be contracting, as four of five in our sample exhibit extended "infall asymmetry" in the CS 2-1 transition millimeter wave transition (Lee, Myers, and Tafalla 2001). Based on the location of the detected stellar objects in the J - H vs. H - K_s color-color plane, no substantial evidence for an association with embedded young stellar objects is found. These cores are found to have mean extinction lower limits of between $A_v = 10 \pm 20$ with individual positions showing minimum extinctions as high as $A_v = 46$. The extinctions we measure are only lower limits and underestimate the true core extinctions which might exceed $A_v = 50$ in some cases. These extinctions are significantly higher than typical dark clouds or globules such as B68 determined either from optical or NIR surveys, but are consistent with submillimeter continuum surveys of starless prestellar cores. An analysis of individual cloud extinctions show column density contrasts of 1.5 - 34 over scales of 0.05 pc. A statistical

analysis of our extinctions for L1709A and L1582A show that the data are consistent with the A_V A_V relationship of Lada, Alves, and Lada (1999b) and Alves et al. (1998) tentatively indicating the presence of a smooth and systematic density distribution at scales lengths less than a core size. By comparing our observations to theoretical studies, our cores are shown to be free from associated stars down to the H-burning limit and free from brown dwarfs down to $10M_{Jup}$.

We thank Chang Won Lee for assistance with the observations. We thank the staffs of Las Campanas and Palomar observatories for their assistance. We thank Eric Persson for supplying the data reduction scripts and providing invaluable advice on the data reduction process. Phil Myers gratefully acknowledges support from NASA grant NAG 5-6266.

R E F E R E N C E S

Aspin, C., Sandell, G., and Russell, A. P. G. 1994, *A & AS*, 106, 165

Alves, J., Lada, C. J., and Lada, E. A. 2001, *Nature*, 409, 159

Alves, J., Lada, C. J., Lada, E. A., Kenyon, S. J., Phelps, R. 1998, *ApJ*, 506, 292

Beichman, C. A., Myers, P. C., Emerson, J. P., Harris, S., Mathieu, R., Benson, P. J., and Jennings, R. E. 1986, *ApJ*, 307, 337

Benson, P. J., and Myers, P. C. 1989, *ApJS*, 71, 89

Bertin, E., and Arnouts, S. 1996, *A & AS*, 117, 393

Bohlin, R. C., Savage, B. D., and Drake, J. F. 1978, *ApJ*, 224, 132

Bontemps, S., Andre, P., Terebey, S., and Cabrit, S., *A & A*, 311, 858

Cernicharo, J., and Bachiller, R. 1984, *A & AS*, 58, 327

Chandler, C. J., Barsony, M., and Moore, T. J. T. 1998, *MNRAS*, 299, 789

Elias, J. H. 1978, *ApJ*, 224, 453

Elias, J. H. 1978, *ApJ*, 224, 857

Evans, N. J. 1999, *ARA & A*, 37, 311

Gardel, G. L., Strom, K. M., and Strom, S. E. 1973, *ApJ*, 184, L53

G regerson, E M ., Evans, N J., Zhou, S ., and Choi, M . 1997, *ApJ*, 484, 256

H yland, A R . 1981, A R ., in IAU Symposium No. 96, *Infrared Astronomy*, ed. C G .W ynn-W illiams and D P .C ruitshank (D ordrecht: Reidel), 125

H ummer, D ., and Rybicki G B . 1968, *ApJ*, 153, L107

Jijina, J., Myers, P C ., and Adams, F C . 1999, *ApJS*, 125, 161

K ram er, C ., A lves, J., Lada, C J., Lada, E A ., Sievers, A ., U ngeredts, H ., and W almsley, C M . 1999, *A&A*, 342, 257

K oomneef, J. 1983, *A&A*, 128, 84

Lada, E A . 1990, Ph D . Thesis, The University of Texas, 1990

Lada, C J., and Adams 1992, F C . 1992, *ApJ*, 393, 278

Lada, E A . 1998, in *Origins*, ASP Conference Series, 148, 198

Lada, C J., A lves, J., and Lada, E A . 1999, in *The Physics and Chemistry of the Interstellar Medium*, Proceedings of the 3rd Cologne-Zermatt Symposium, ed. V .O ssenkopf and G .W innewisser, GCA-Verlag Herdecke, 161

Lada, C J., A lves, J., and Lada, E A . 1999, 512, 250

Lada, C J., Lada, E A ., Clemens, D P ., and Bally, J. 1994, *ApJ*, 429, 694

Lee, C W ., and Myers, P C ., F C . 1999, *ApJS*, 123, 233

Lee, C W ., Myers, P C ., and Tafalla, M . 2001, *ApJS*, 136, 703

M ardones, D ., Myers, P C ., Tafalla, M ., W ilner, D J., Bachiller, R ., and Garay, G . 1997, *ApJ*, 489, 719

M urphy, D C ., Persson, S E ., Pahre, M A ., Sivaramakrishnan, A ., and Djorgovski, S G . 1995, *PAASP*, 107 1234

M yers, P C ., Linke, R A ., and Benson, P C . 1983, *ApJ*, 264, 517

M yers, P C ., Bachiller, R ., Caselli, P ., Fuller, G A ., M ardones, D ., Tafalla, M ., and W ilner, D J. 1995, *ApJ*, 449, L65

Persson, S E ., Murphy, D C ., Krzeminski, W ., Roth, M ., and Reike, M J. 1998, *AJ*, 116, 2475

Rubio, M., Barba, R. H., Walbom, N. R., Robst, R. G., Garcia, J., and Roth, M. R. 1998, *AJ*, 116, 1708

Visser, A. E., Richter, J. S., and Chandler, C. J. 2001, *MNRAS*, 323, 257

Ward-Thompson, D., Motte, F., and Andre, P. 1999, *MNRAS*, 305, 143

Weintraub, D. A., Saumon, D., Kastner, J. H., Forveille, T. 2000, *ApJ*, 530, 867

Wilkling, B. A. 1997, in *Origins of Life and Evolution of the Biosphere*, 27, Issue 1/3, 135

Zhou, S., Evans, N. J., Kompe, C., and Walsley, C. M. 1993, *ApJ*, 404, 232

Zhou, S., Evans, N. J., Peng, R., and Lo, K. Y. 1994, *ApJ*, 433, 131

Zinnecker, H., McCaughrean, M. 1991, *Mem. Soc. Astron. It.*, 62, 761

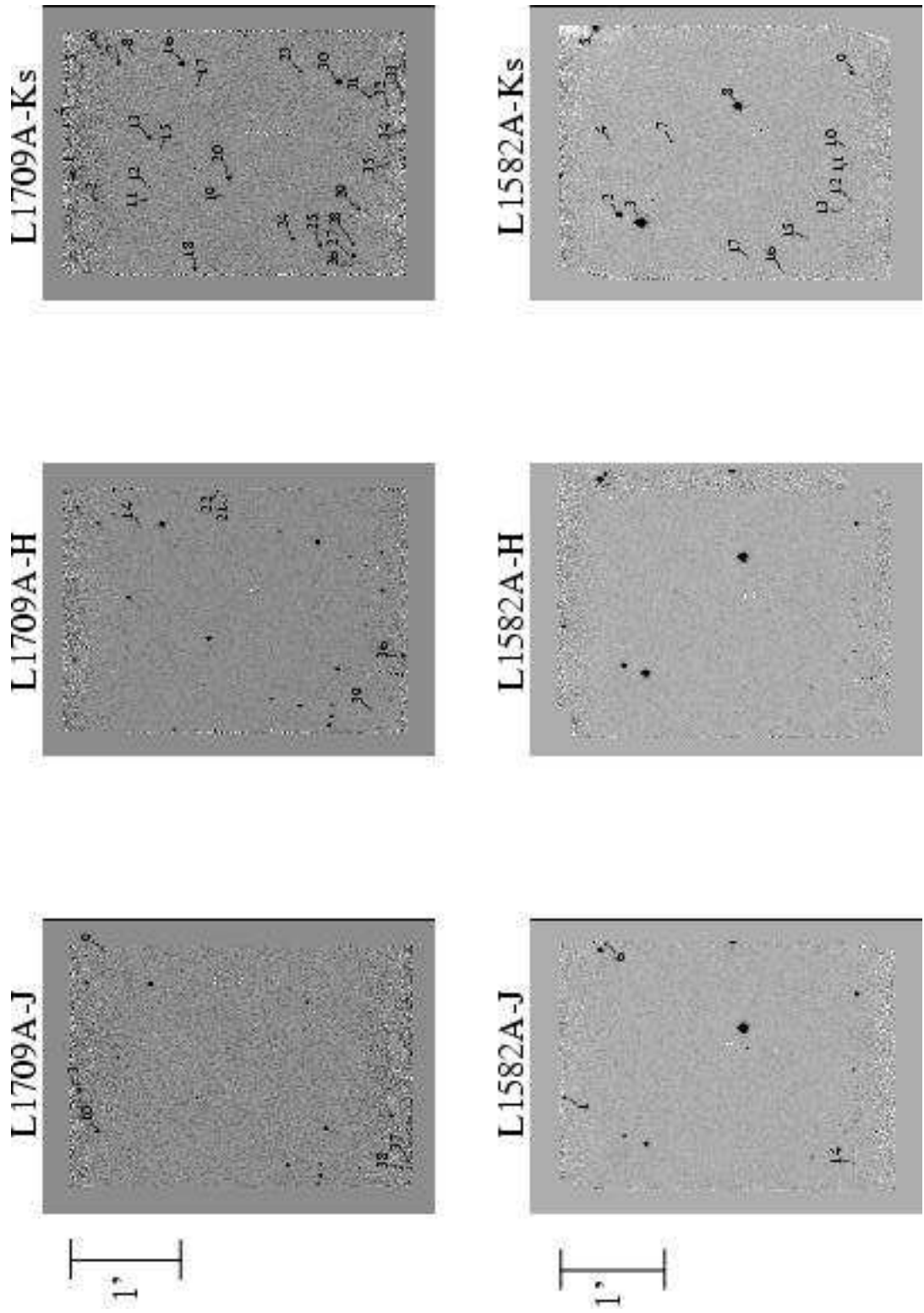


Fig. 1. JH K_s mosaics of L1709A and L1582A

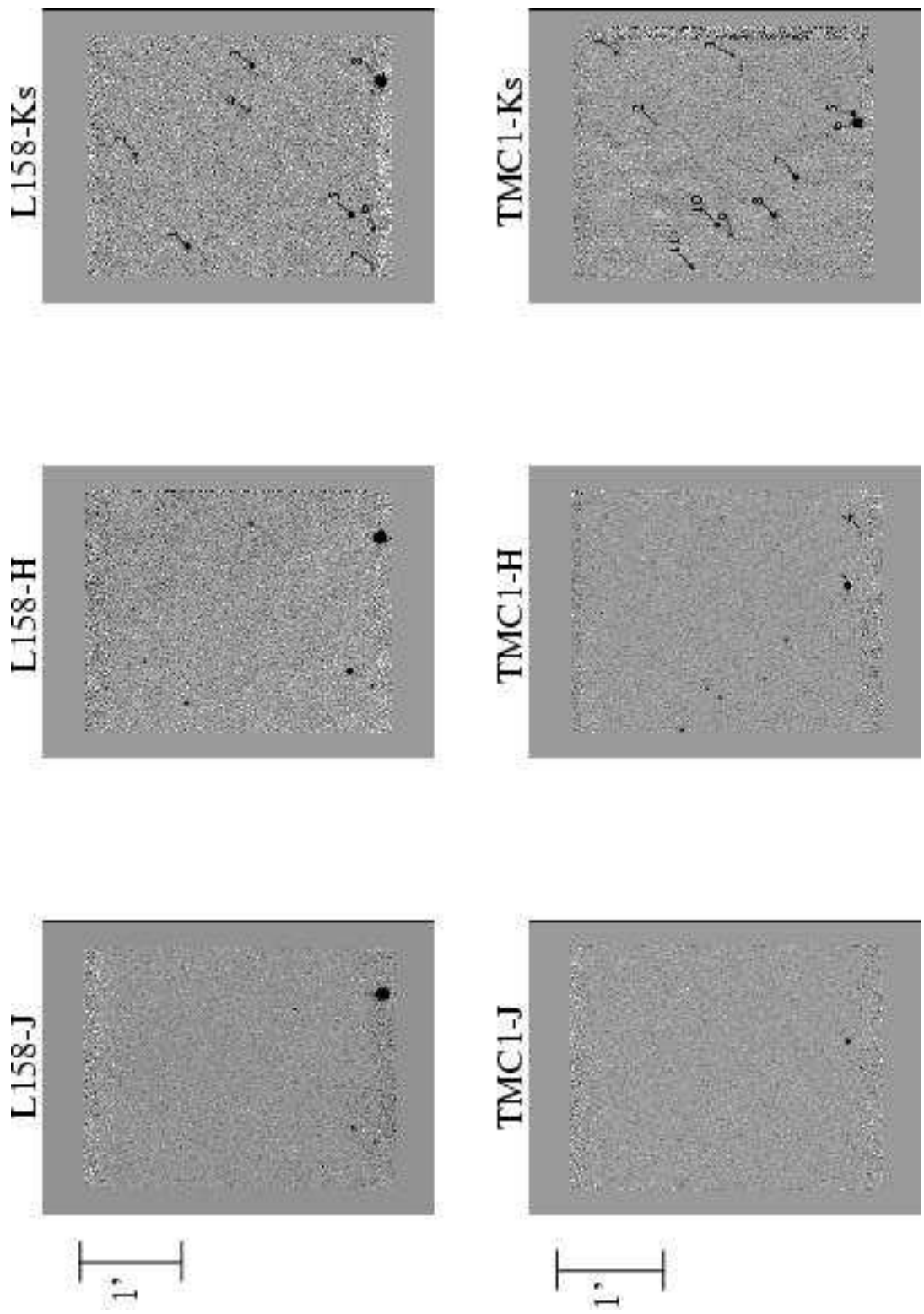


Fig. 2. | JH K_s mosaics of L158 and TMC1

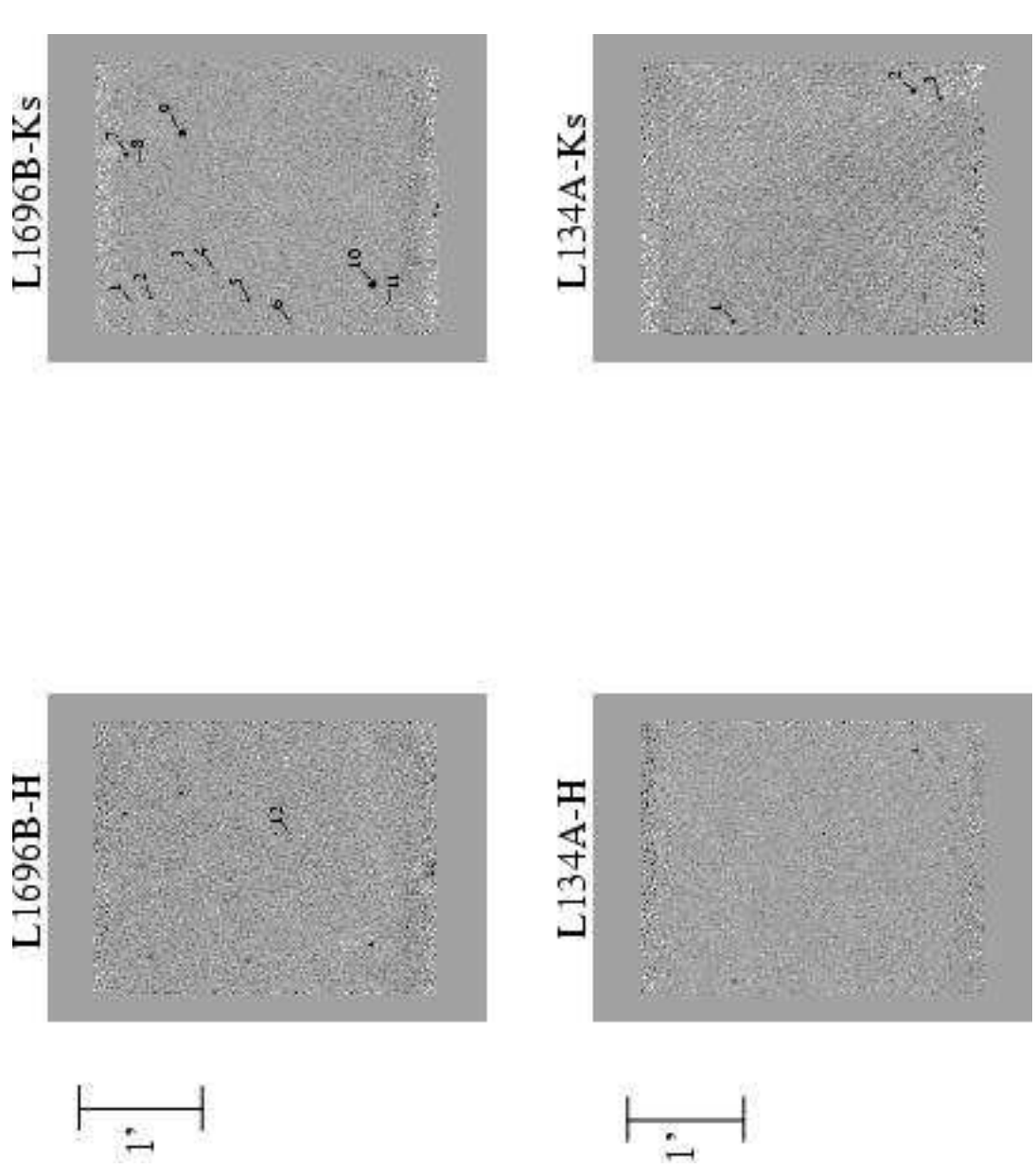


Fig. 3. | H K_s mosaics of L1696B and L134A

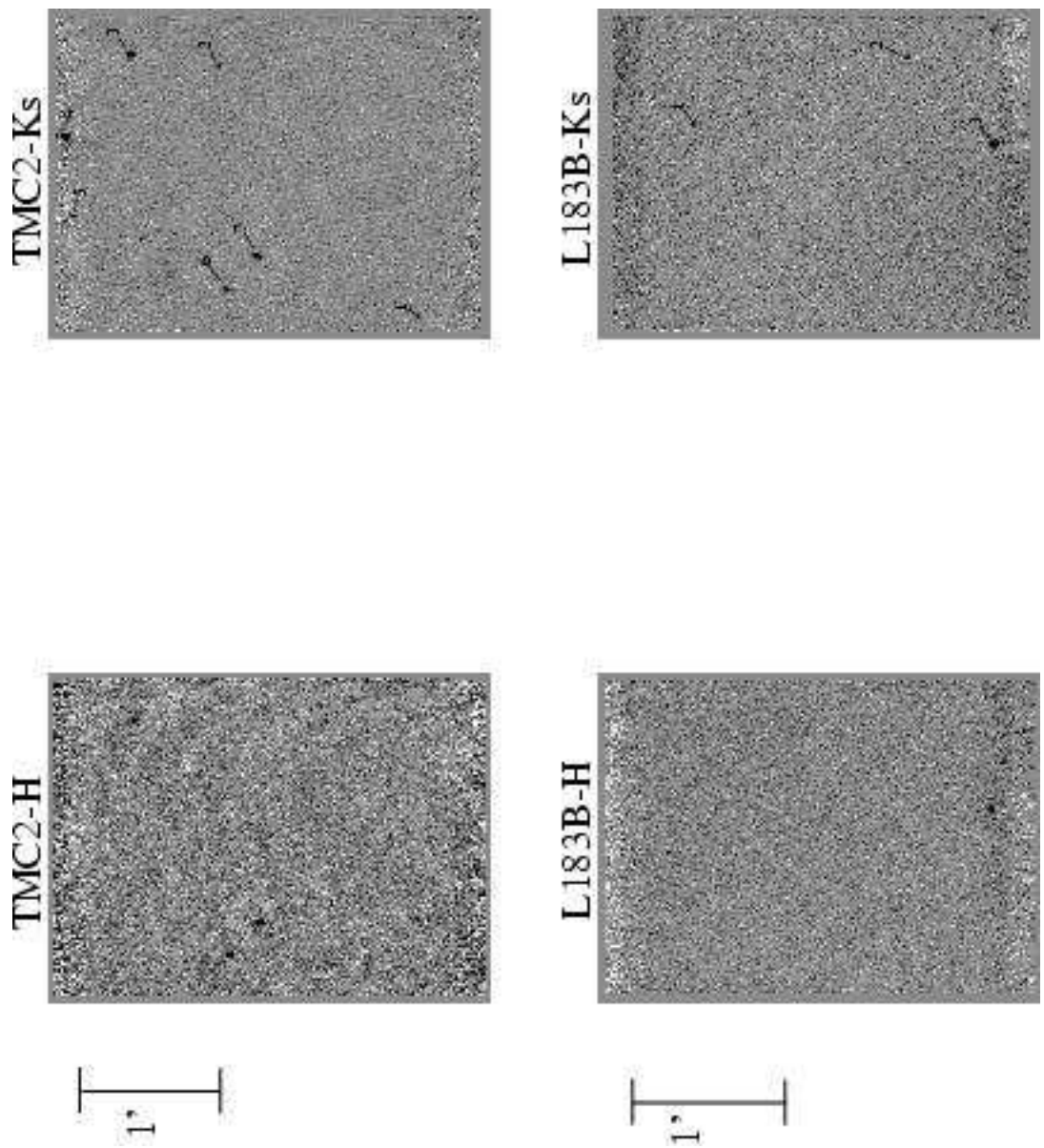


Fig. 4. | H K_s mosaics of TMC2 and L183B

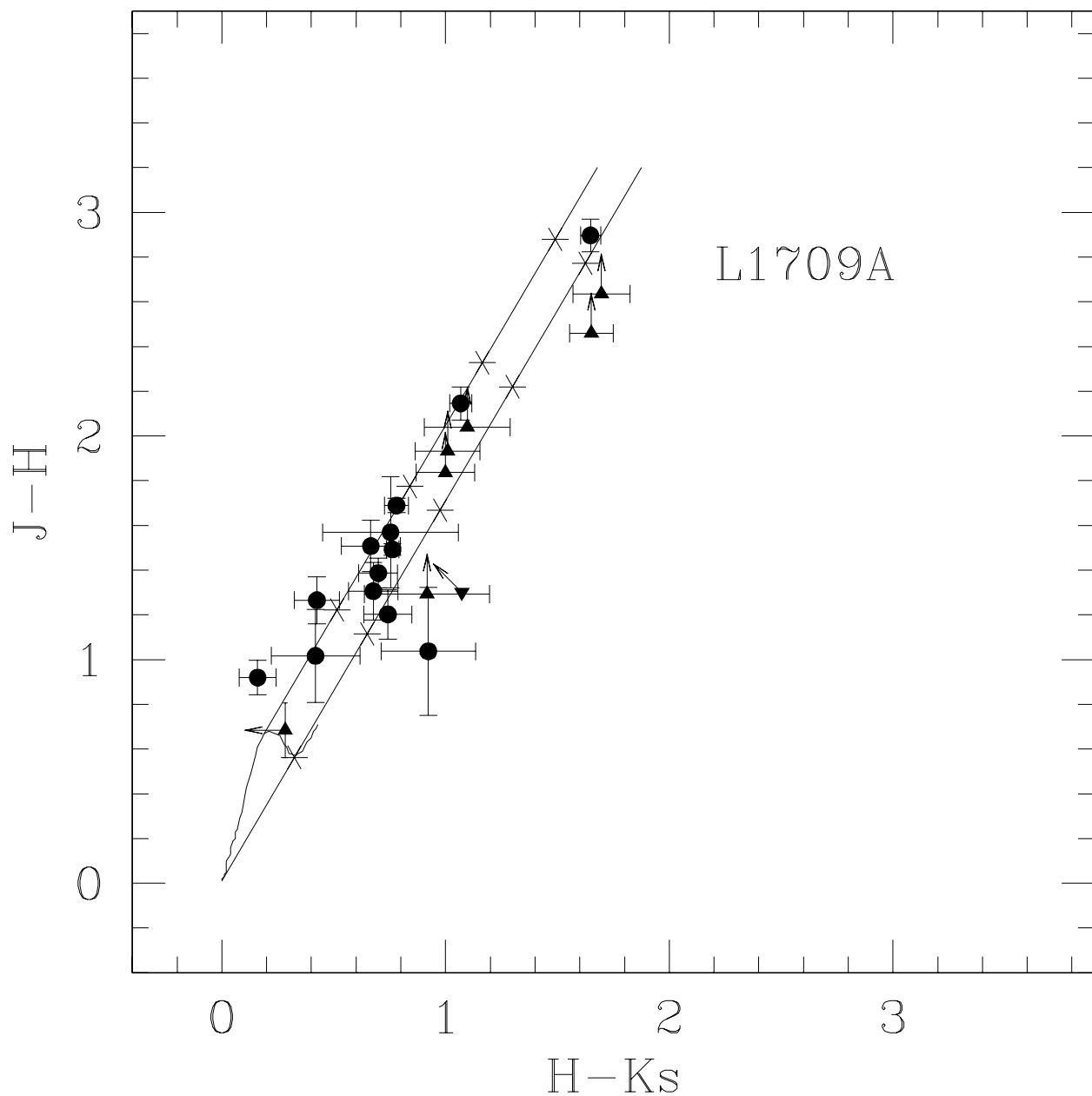


Fig. 5.1 Color-color plot for L1709A .

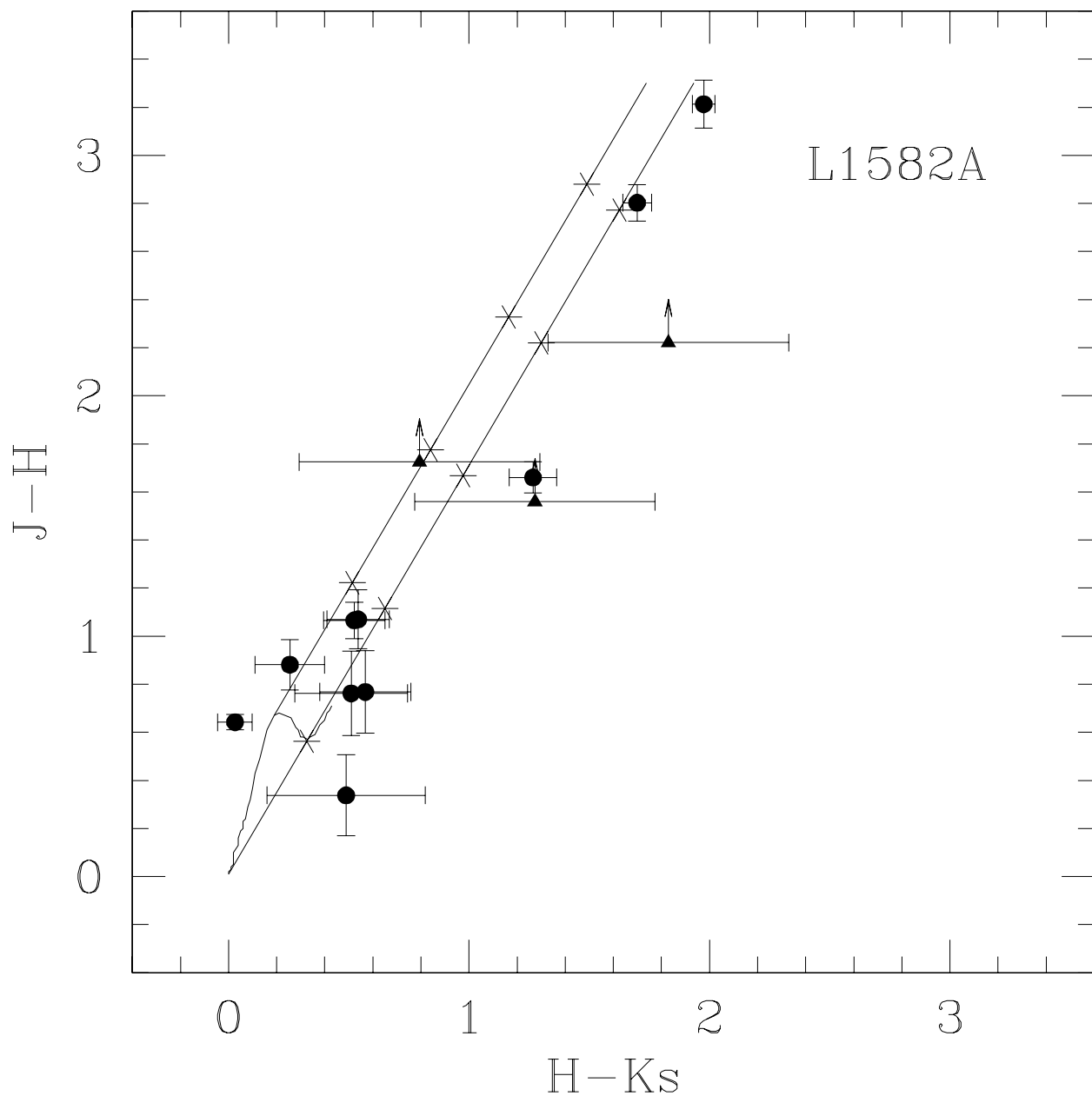


Fig. 6. | Color-color plot for L1582A .

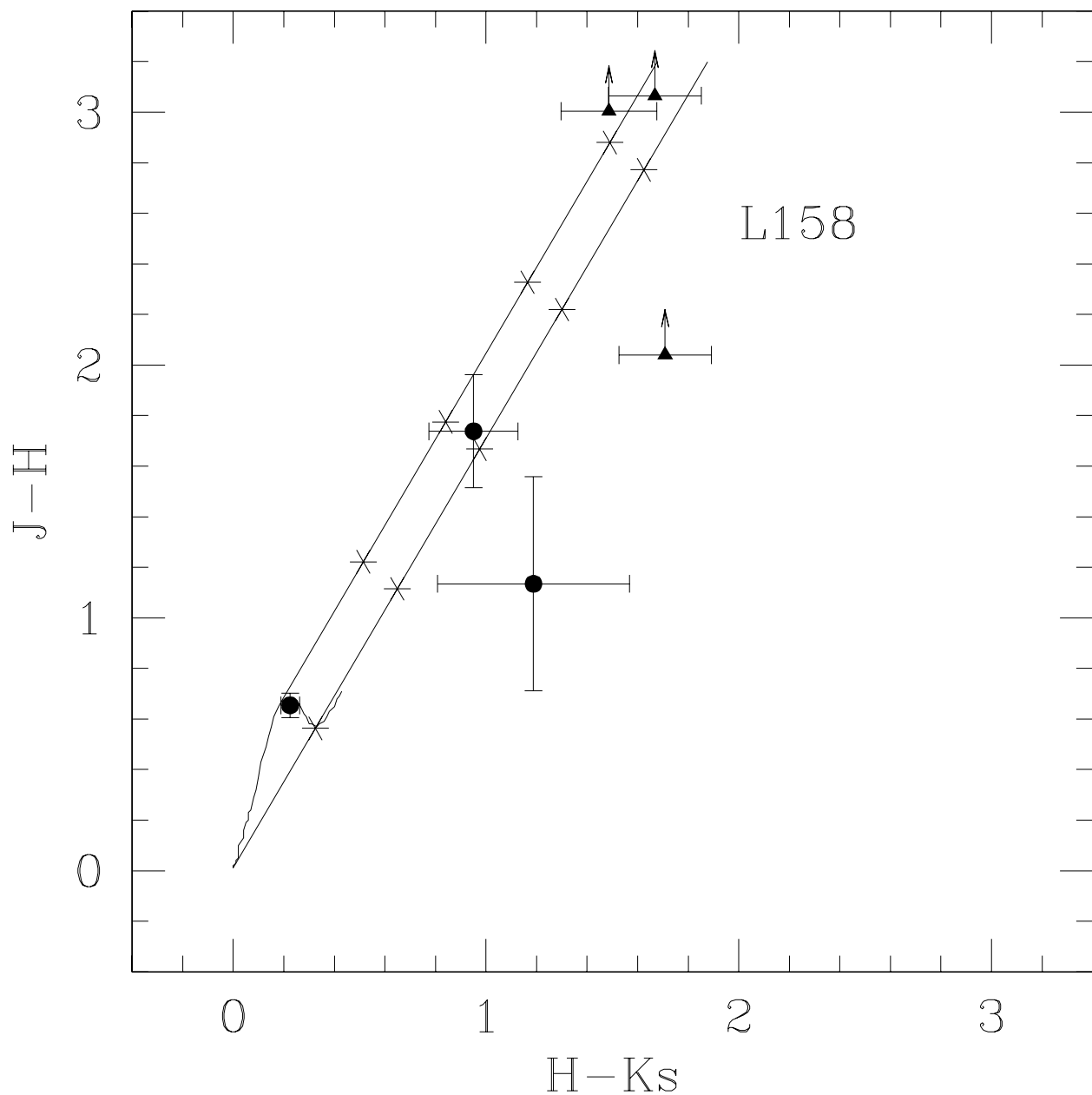


Fig. 7.1 Color-color plot for L158.

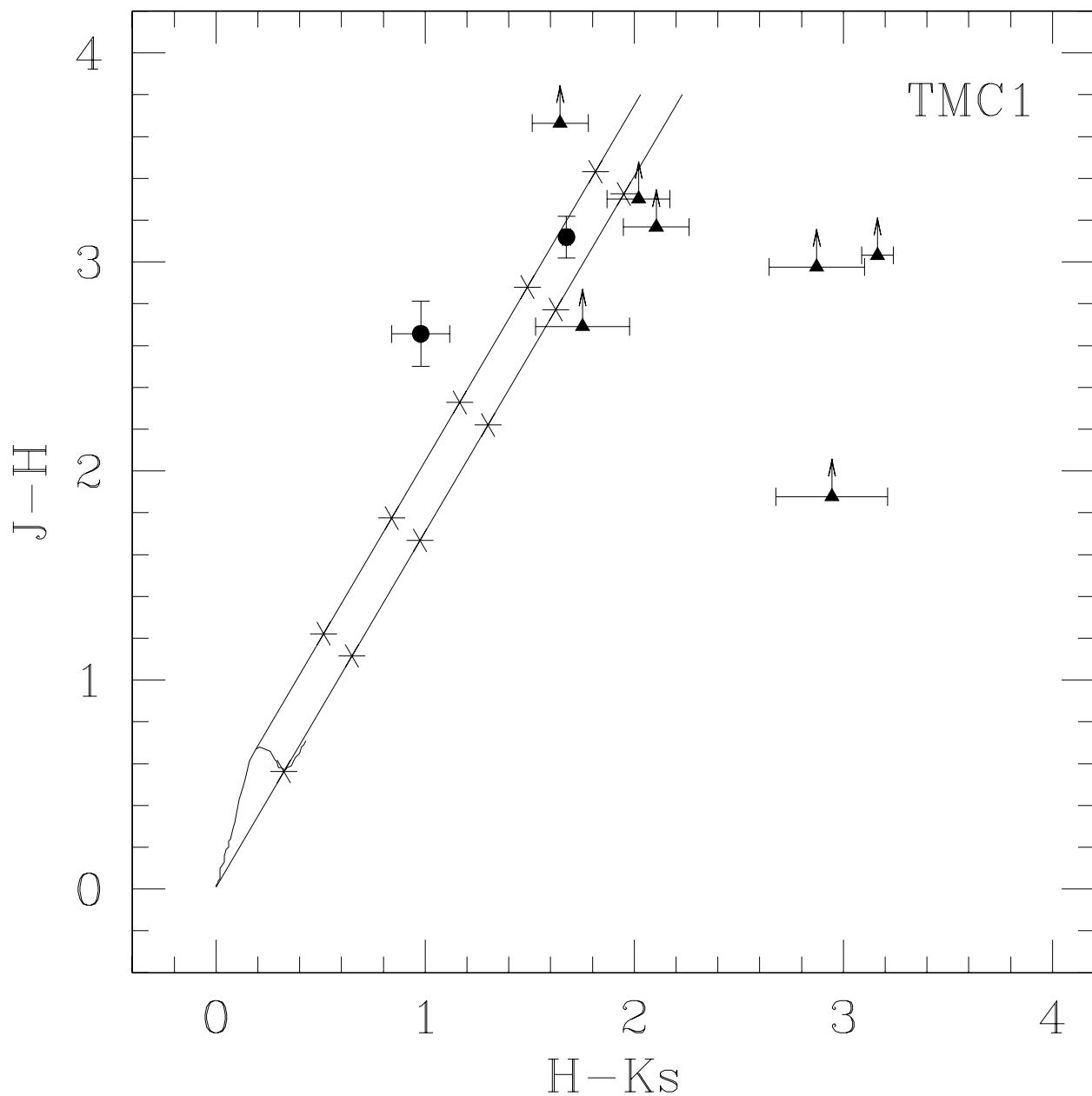


Fig. 8.1 Color-color plot for TMC 1.

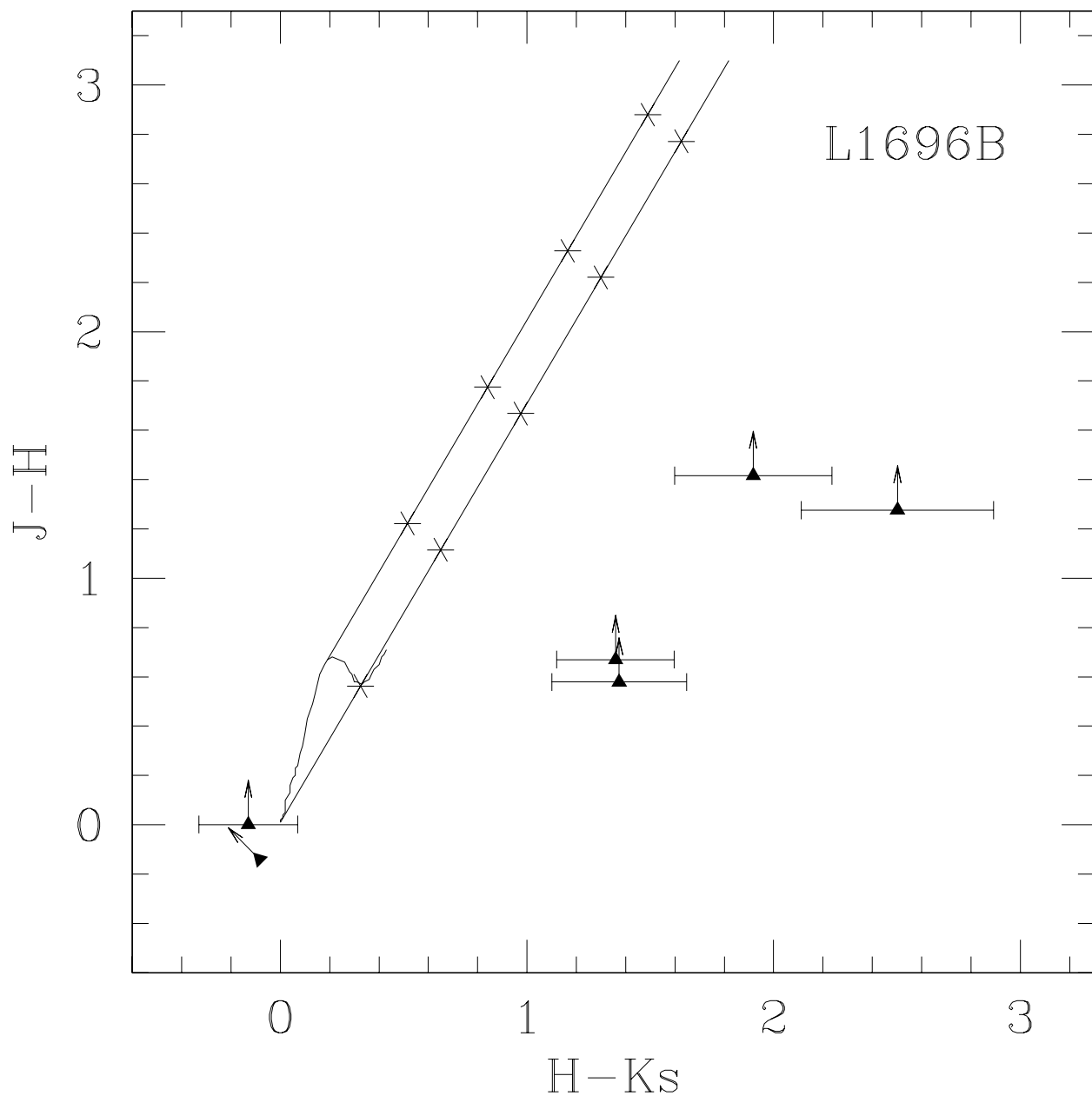


Fig. 9. | Color-color plot for L1696B .

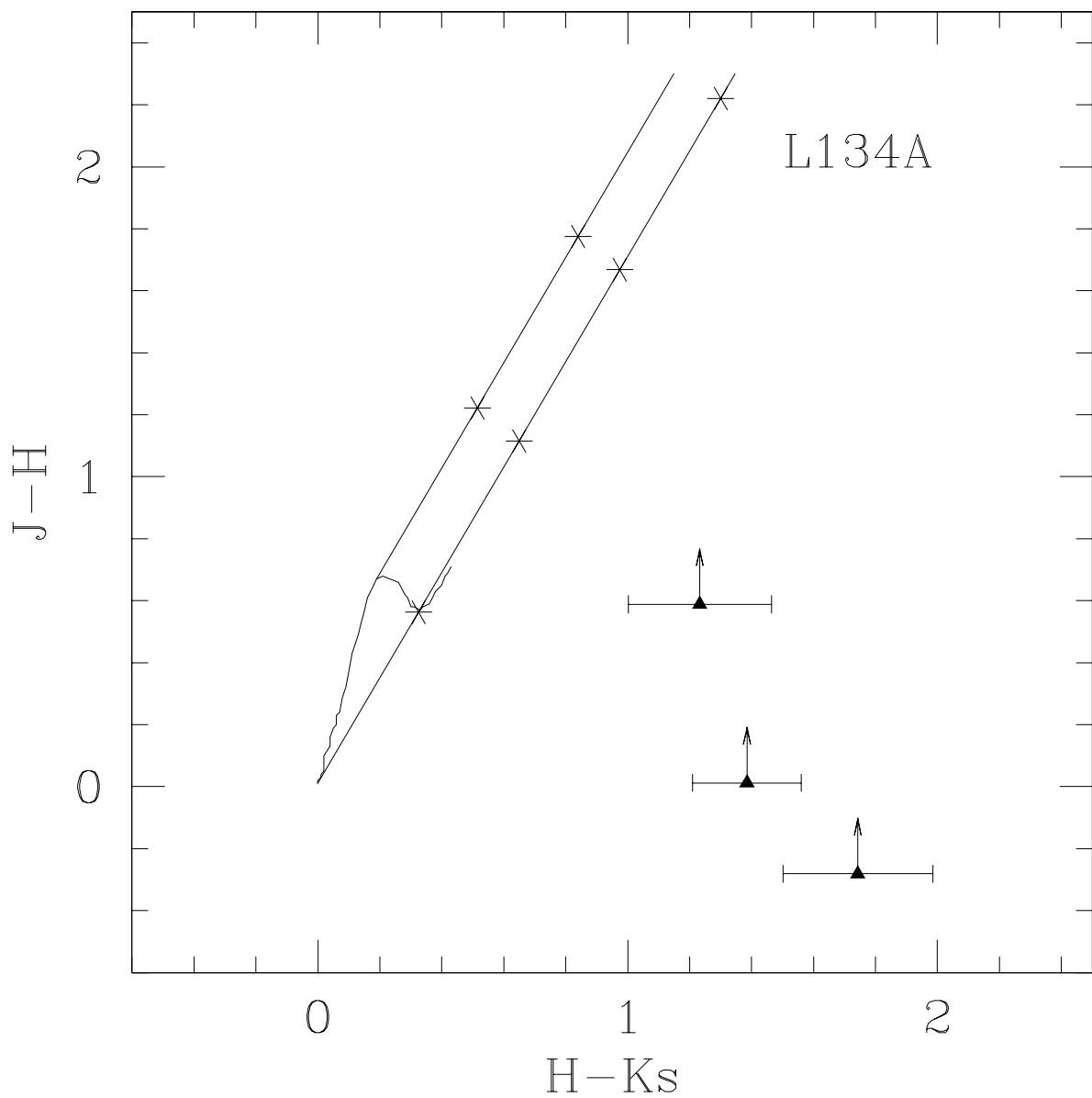


Fig. 10. | Color-color plot for L134A .

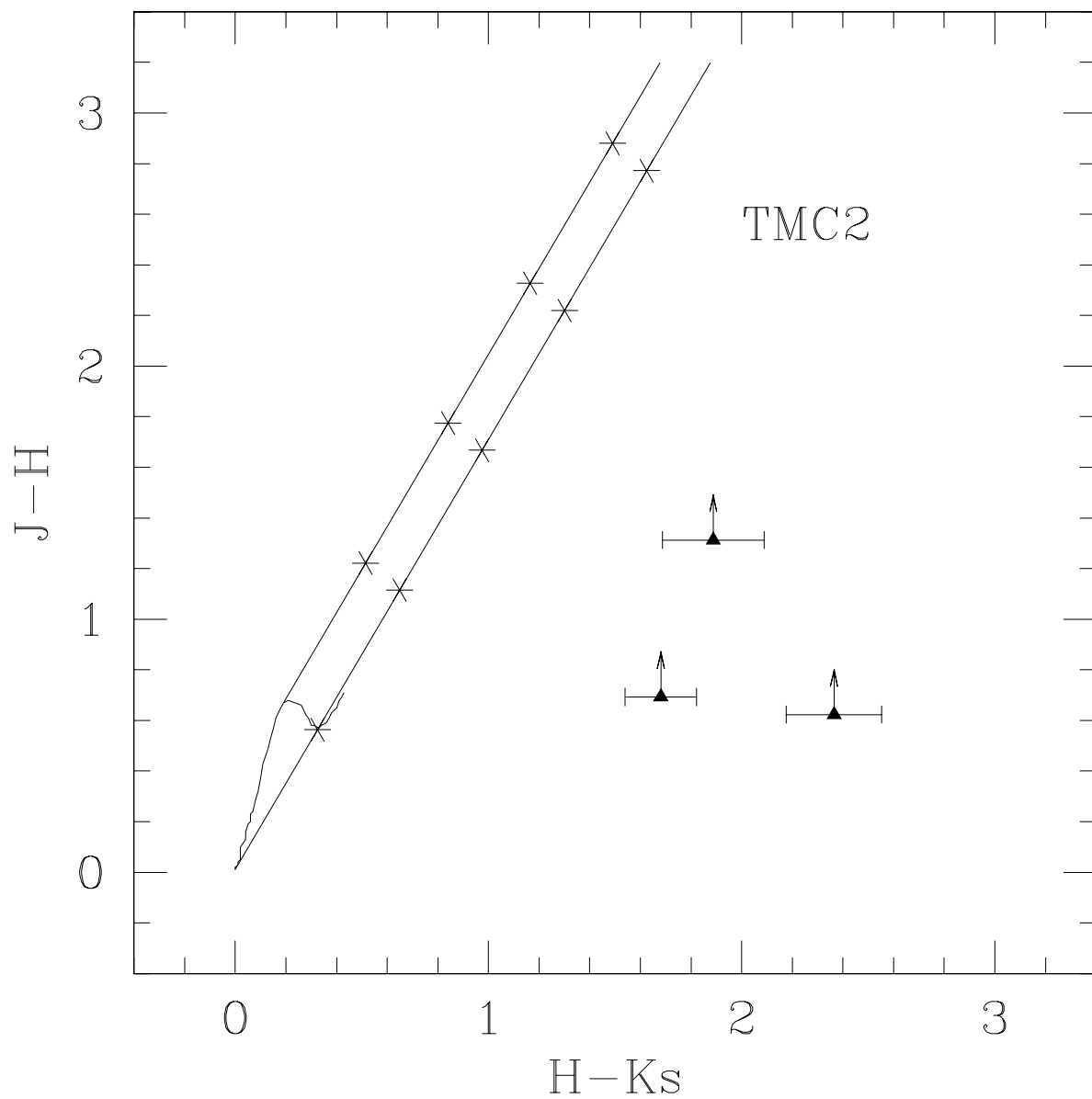


Fig. 11.1 Color-color plot for TMC2.

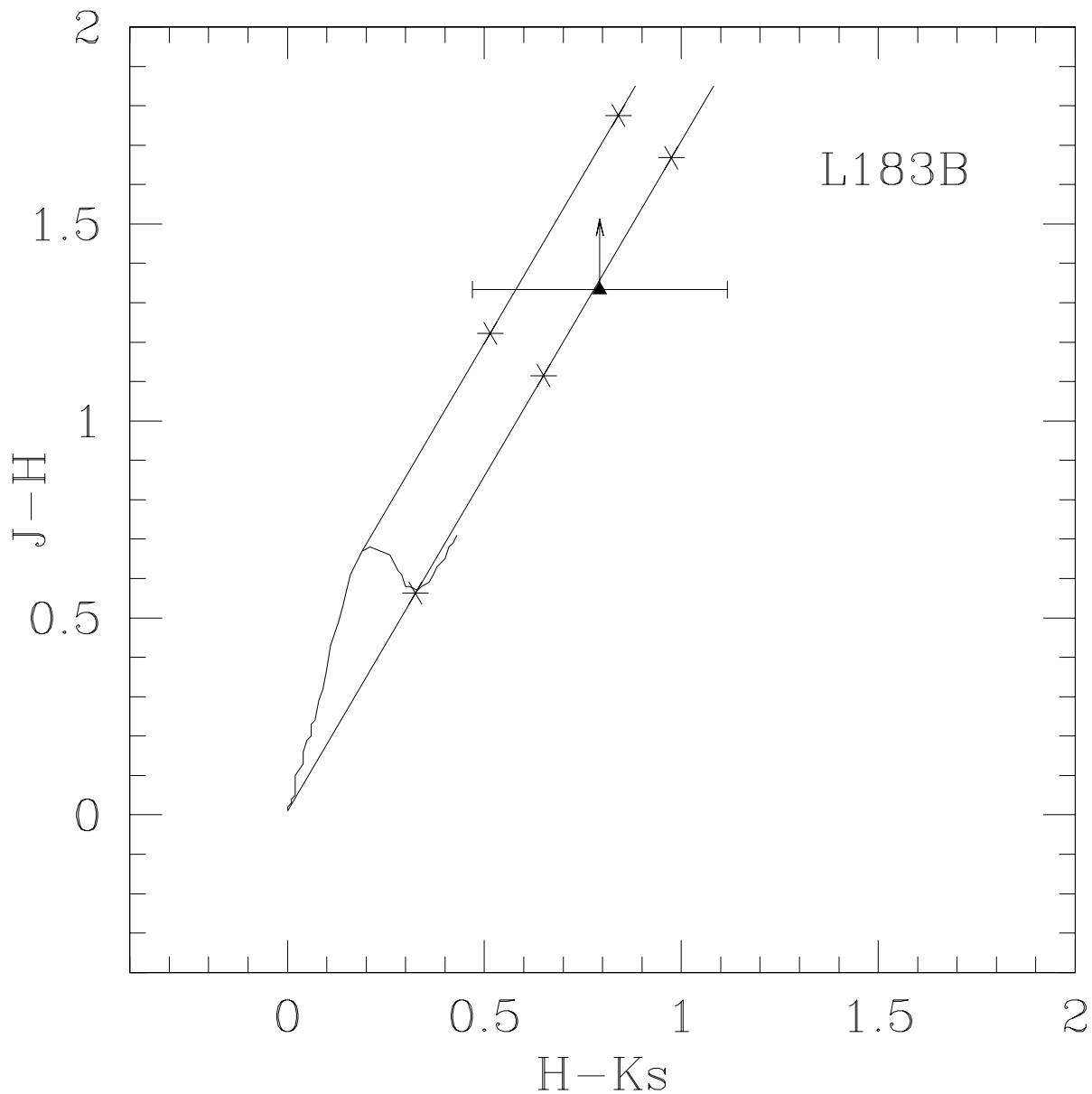


Fig. 12. | Color-color plot for L183B .

Table 1. Observational parameters.

Run	U T Dates	Telescope	Camera Plate Scale (arcsec pixel ⁻¹)	Camera F O V (arcmin)
1	6/17/97 - 6/23/97	LCO 1 m	0.60	2.56 X 2.56
2	11/6/97 - 11/8/97	Pal 1.5 m	0.62	2.65 X 2.65
3	3/17/98 - 3/19/98	LCO 1 m	0.60	2.56 X 2.56

Table 2. Starless dense core field centers.

Core Name	R A. (J2000.0)	D ecl. (J2000.0)	Position Reference	Est. Pos. Error (arcsec)	Run
L1709A	16 30 50.8	-23 41 53.0	a	10	3
L1582A	5 32 00.3	12 30 28.2	a	10	3
L158	16 47 23.2	-13 59 21.1	a	10	1
TM C 1	4 41 33.0	25 44 44.0	b	5	2
L1696B	16 28 59.3	-24 20 43.0	a	10	1
L134A	15 53 36.4	-4 35 26.0	a	10	1
TM C 2	4 32 48.7	24 25 12.0	b	5	2
L183B	15 54 06.5	-2 51 39.0	b	10	1

^aBenson and Myers (1989). Also, see text.

^bLee, Myers, and Tafalla (2001)

Table 3. Magnitudes and colors for identified L1709A stars.

Star	J	H	K _s	J	H	H	K _s	A _V (K 5)
1	o fram e	o fram e	15:037 0:090	:::		:::		:::
2	o fram e	17:752 0:133	16:660 0:354	:::		1:092 0:378		14:339
3	17:692 0:065	> 19:262	> 17:868	< 1:570		:::		:::
4	o fram e	o fram e	15:402 0:106	:::		:::		:::
5	o fram e	o fram e	16:818 0:166	:::		:::		:::
6	o fram e	16:990 0:127	16:346 0:109	:::		0:644 0:167		7:446
7	17:626 0:042	16:360 0:096	15:935 0:027	1:266 0:105	0:425 0:100			4:077
8	19:172 0:160	18:155 0:133	17:736 0:147	1:017 0:208	0:419 0:198			3:985
9	18:741 0:092	17:425 0:113	o fram e	1:316 0:146		:::		:::
10	17:937 0:145	> 19:262	> 17:868	< 1:325		:::		:::
11	19:783 0:244	18:746 0:149	17:823 0:149	1:037 0:286	0:923 0:211			11:739
12	20:157 0:235	18:588 0:082	17:834 0:149	1:569 0:249	0:754 0:304			9:139
13	17:781 0:047	16:394 0:048	15:695 0:073	1:387 0:067	0:699 0:087			8:293
14	> 20:243	18:941 0:174	> 17:868	> 1:302	< 1:073			:::
15	> 20:243	18:406 0:095	17:407 0:090	> 1:837	0:999 0:131			12:908
16	16:359 0:019	14:866 0:007	14:103 0:016	1:493 0:020	0:763 0:017			9:277
17	> 20:243	18:311 0:111	17:302 0:094	> 1:932	1:009 0:145			13:062
18	o fram e	16:840 0:054	16:021 0:026	:::	0:819 0:060			10:139
19	> 20:243	18:950 0:127	18:033 0:250	> 1:293	0:917 0:280			11:646
20	18:254 0:063	16:108 0:036	15:040 0:026	2:146 0:073	1:068 0:044			13:970
21	> 20:243	18:337 0:102	:::	> 1:906	:::			:::
22	19:462 0:172	17:918 0:103	o fram e	1:544 0:200	:::			:::
23	> 20:243	17:784 0:073	16:132 0:064	> 2:459	1:652 0:097			22:954
24	:::	17:358 0:155	16:286 0:044	:::	1:072 0:161			14:031
25	18:285 0:040	16:777 0:108	16:111 0:075	1:508 0:115	0:666 0:131			7:785
26	17:941 0:060	17:021 0:049	16:861 0:067	0:920 0:077	1:600 0:083			0:000
27	17:872 0:072	16:566 0:106	15:889 0:027	1:306 0:128	0:677 0:109			7:954
28	18:520 0:063	17:318 0:091	16:576 0:059	1:202 0:111	0:742 0:108			8:954
29	17:761 0:028	16:072 0:007	15:291 0:050	1:689 0:029	0:781 0:050			9:554
30	18:387 0:061	15:490 0:041	13:842 0:009	2:897 0:073	1:648 0:042			22:893
31	> 20:243	17:608 0:111	15:911 0:064	> 2:635	1:697 0:128			23:647
32	> 20:243	18:204 0:153	17:107 0:116	> 2:039	1:097 0:192			14:416
33	> 20:243	16:701 0:066	15:406 0:098	> 3:542	1:295 0:118			17:462
34	:::	16:972 0:064	15:763 0:081	:::	1:209 0:103			16:139
35	> 20:243	18:064 0:139	16:588 0:085	> 2:179	1:476 0:163			20:247
36	16:926 0:017	15:587 0:189	o fram e	1:339 0:190	:::			:::
37	17:438 0:046	o fram e	o fram e	:::	:::			:::
38	18:700 0:153	o fram e	o fram e	:::	:::			:::
39	18:835 0:088	18:151 0:085	> 17:868	0:684 0:122	< 0:283			:::

Table 4. Magnitudes and colors for identified L1582A stars.

Star	J	H		K _s		J	H	H	K _s	A _V (K 5)
1	16:187	0:97	14:735	0:048	o frame	1:452	0:108	---	---	---
2	16:837	0:068	14:034	0:018	12:335	0:035	2:803	0:070	1:699	0:039
3	15:502	0:094	12:289	0:024	10:313	0:001	3:213	0:097	1:976	0:024
4	> 19:280		17:721	0:153	16:447	0:113	> 1:559	1:274	0:190	17:139
5	14:766	0:012	13:106	0:059	11:840	0:071	1:660	0:060	1:266	0:092
6	16:162	0:153	14:982	0:138	o frame	1:180	0:206	---	---	---
7	> 19:280		17:059	0:095	15:230	0:117	> 2:221	1:829	0:151	25:678
8	12:070	0:001	11:428	0:001	11:401	0:033	0:642	0:001	0:027	0:033
9	15:577	0:040	14:511	0:060	13:988	0:112	1:066	0:072	0:523	0:127
10	17:429	0:078	16:548	0:070	16:293	0:127	0:881	0:105	0:255	0:145
11	17:426	0:124	17:088	0:114	16:599	0:310	0:338	0:168	0:489	0:330
12	17:195	0:044	16:433	0:169	15:923	0:162	0:762	0:175	0:510	0:234
13	17:761	0:156	16:993	0:073	16:424	0:174	0:768	0:172	0:569	0:189
14	17:831	0:112	> 18:119		> 17:170		< 0:288	---	---	---
15	17:797	0:113	16:727	0:049	16:188	0:128	1:070	0:123	0:539	0:137
16	o frame		16:803	0:077	16:138	0:059	---	0:665	0:097	7:769
17	> 19:280		17:555	0:102	16:761	0:137	> 1:725	0:794	0:171	9:754

Table 5. Magnitudes and colors for identified L158 stars.

Star	J	H		K _s		J	H	H	K _s	A _V (K 5)	
1	> 19.999	16.934	0.180	15.266	0.040	> 3.065		1.668	0.184	23.201	
2	> 19.999	17.959	0.146	16.250	0.110	> 2.040		1.709	0.183	23.831	
3	> 19.999	16.995	0.147	15.509	0.119	> 3.004		1.486	0.189	20.400	
4	> 19.999	> 18.577		16.186	0.081	:::		> 2.391		34.324	
5	17.496	0.190	15.758	0.118	14.807	0.130	1.738	0.224	0.951	0.176	
6	18.343	0.253	17.208	0.340	16.020	0.170	1.135	0.424	1.188	0.380	
7	19.375	0.234	> 18.577		> 17.616		< 0.798	:::		:::	
8	12.738	0.001	12.084	0.001	11.859	0.003	0.654	0.001	0.225	0.003	1.000

Table 6. Magnitudes and colors for identified TM C1 stars. The K_s lower limit is 19.842.

Star	J	H		K_s		J	H	H	K_s	A_V (K_s)
1	> 21:396	19:519	0:224	16:574	0:145	> 1:877	2:945	0:267	42:847	
2	> 21:396	> 19:889		17:515	0:078	:::	:::	:::	:::	
3	> 21:396	18:705	0:143	16:952	0:174	> 2:691	1:753	0:225	24:508	
4	> 21:396	18:746	0:146	o frame		> 2:650	:::	:::	:::	
5	> 21:396	17:732	0:093	16:086	0:097	> 3:664	1:646	0:134	22:862	
6	17:741 0:089	14:622	0:003	12:946	0:002	3:119 0:089	1:676	0:004	23:324	
7	> 21:396	18:364	0:073	15:200	0:022	> 3:032	3:164	0:076	46:217	
8	> 21:396	18:420	0:217	15:547	0:071	> 2:976	2:873	0:228	41:740	
9	> 21:396	18:229	0:093	16:124	0:125	> 3:167	2:105	0:156	29:924	
10	> 21:396	18:095	0:114	16:074	0:097	> 3:301	2:021	0:150	28:631	
11	20:398 0:111	17:742	0:110	16:763	0:085	2:656 0:156	0:979	0:139	12:600	

Table 7. Magnitudes and colors for identified L1696B stars.

Star	J	H	K _s	J	H	H	K _s	A _V (K 5)
1	> 18:039	> 18:616	17:619	0:294	:::	> 0:997	:::	
2	> 18:039	> 18:616	17:131	0:215	:::	> 1:485	:::	
3	> 18:039	18:038 0:161	18:168	0:120	> 0:001	0:130 0:201	:::	
4	> 18:039	> 18:616	17:773	0:135	:::	> 0:843	:::	
5	> 18:039	17:369 0:209	16:010	0:113	> 0:670	1:359 0:238	18:447	
6	> 18:039	> 18:616	17:866	0:101	:::	> 0:750	:::	
7	> 18:039	17:460 0:249	16:086	0:113	> 0:579	1:374 0:273	18:677	
8	> 18:039	> 18:616	18:200	0:296	:::	> 0:416	:::	
9	> 18:039	16:623 0:319	14:706	0:005	> 1:416	1:917 0:319	27:031	
10	> 18:039	16:763 0:390	14:261	0:008	> 1:276	2:502 0:390	36:032	
11	> 18:039	> 18:616	16:402	0:225	:::	> 2:214	:::	
12	> 18:039	18:178 0:167	> 18:263	> 0:139	< 0:085	:::		

Table 8. Magnitudes and colors for identified L134A stars. The H and K_s lower limits are 20.152 and 19.192, respectively.

Star	J	H	K _s	J	H	H	K _s	A _V (K 5)	
1	> 17:947	17:935	0:163	16:550	0:067	> 0:012	1:385	0:176	18:847
2	> 17:947	17:359	0:147	16:126	0:178	> 0:588	1:233	0:231	16:508
3	> 17:947	18:228	0:122	16:485	0:209	> 0:281	1:743	0:242	24:354

Table 9. Magnitudes and colors for identified TM C2 stars. The K_s lower limit is 19.152.

Star	J	H	K_s	J	H	H	K_s	A_V (K 5)
1	> 19:329	> 20:113	18:336	0:226	---	> 1:777	---	---
2	> 19:329	> 20:113	17:751	0:069	---	> 2:362	---	---
3	> 19:329	18:706 0:183	16:341	0:043	> 0:623	2:365 0:188	33:924	
4	> 19:329	---	15:576	0:039	---	---	---	---
5	> 19:329	> 20:113	17:192	0:082	---	> 2:921	---	---
6	> 19:329	18:636 0:118	16:955	0:077	> 0:693	1:681 0:141	23:401	
7	> 19:329	18:016 0:157	16:128	0:124	> 1:313	1:888 0:200	26:585	

Table 10. Magnitudes and colors for identified L183B stars. The K_s lower limit is 19.151.

Star	J	H	K_s	J	H	H	K_s	A_V (K 5)
1	> 18:154	> 18:660	17:115	0:207	:::	> 1:545	:::	
2	> 18:154	> 18:660	17:269	0:152	:::	> 1:391	:::	
3	> 18:154	16:821	0:089	16:028	0:312	> 1:333	0:793	0:324

Table 11. Mean extinction measures by core.

Core	$\langle A_V \rangle$
L1709A	12.2
L1582A	11.3
L158	18.7
TM C 1	30.3
L1696B	25.0
L134A	19.9
TM C 2	28.0
L183B	9.7

Table 12. Estimated core density lower limits and sizes.

Core	n_{tot} (cm^{-3})	M (M_{\odot})	$\frac{P}{\text{A}}$ (pc)	Polygon Boundary Definition
L1709A	$5.3 \cdot 10^4$	1.5	0.075	15, 17, 23, 30, 31, 34, 35, 29, 25, 24, 20, 15
L1582A	$1.8 \cdot 10^4$	7.1	0.18	3, 7, 8, 9, 10, 11, 12, 13, 15, 16, 17, 3
L158	$8.1 \cdot 10^4$	2.0	0.072	1, 2, 4, 8, 5, 1
TM C 1	$1.6 \cdot 10^5$	2.6	0.062	2, 3, 5, 6, 7, 8, 9, 10, 11, 2
TM C 2	$5.7 \cdot 10^4$	1.1	0.065	1, 2, 3, 4, 5, 6, 7, 1
L1696B	$5.1 \cdot 10^4$	1.0	0.066	1, 8, 7, 9, 10, 11, 6, 5, 4, 3, 2, 1

Table 13. Results of simple model giving absolute magnitude detection limits to core centers

Core	M _K
L1709A	11.2
L1582A	8.7
L158	10.7
TM C 1	12.7
L1696B	11.0
L134A	13.3
TM C 2	12.1
L183B	13.7